Real-Time Probing of Electron Dynamics Using Attosecond Time-Resolved Spectroscopy

Krupa Ramasesha,[1,2] Stephen R. Leone,[1,3,4] and Daniel M. Neumark[1,4]

[1]Department of Chemistry, University of California, Berkeley, California 94720; email: dneumark@berkeley.edu

[2]Combustion Research Facility, Sandia National Laboratories, Livermore, California 94550

[3]Department of Physics, University of California, Berkeley, California 94720

[4]Chemical Sciences Division, Lawrence Berkeley National Laboratory, Berkeley, California 94720

Annu. Rev. Phys. Chem. 2016. 67:41–63

First published online as a Review in Advance on February 24, 2016

The *Annual Review of Physical Chemistry* is online at physchem.annualreviews.org

This article's doi: 10.1146/annurev-physchem-040215-112025

Keywords

ultrafast spectroscopy, electron dynamics, high harmonic generation, transient absorption, photoelectron spectroscopy

Abstract

Attosecond science has paved the way for direct probing of electron dynamics in gases and solids. This review provides an overview of recent attosecond measurements, focusing on the wealth of knowledge obtained by the application of isolated attosecond pulses in studying dynamics in gases and solid-state systems. Attosecond photoelectron and photoion measurements in atoms reveal strong-field tunneling ionization and a delay in the photoemission from different electronic states. These measurements applied to molecules have shed light on ultrafast intramolecular charge migration. Similar approaches are used to understand photoemission processes from core and delocalized electronic states in metal surfaces. Attosecond transient absorption spectroscopy is used to follow the real-time motion of valence electrons and to measure the lifetimes of autoionizing channels in atoms. In solids, it provides the first measurements of bulk electron dynamics, revealing important phenomena such as the timescales governing the switching from an insulator to a metallic state and carrier-carrier interactions.

1. INTRODUCTION

High harmonic generation (HHG): a method by which attosecond bursts of light are generated

XUV: extreme ultraviolet

Physical and chemical processes in nature are governed by a complex interplay of electronic, atomic, and molecular motion. Following these dynamic processes in real time requires sufficient time resolution to sample the signatures of these motions (1). Whereas nuclear motion occurs on a femtosecond timescale—the H–H bond vibration, for example, exhibits a period of 7.5 fs—electron dynamics occur on attosecond timescales. An often used classical but intuitive picture is that of an electron in its ground state orbiting a hydrogen nucleus, which is calculated to have a period of ∼150 as. A metal such as copper serves as the condensed-phase example: An electron traveling in the conduction band at the Fermi velocity (2) can traverse a distance equal to its lattice constant in ∼230 as. Correlation-driven electrons and holes in polyatomic molecules or widely spaced electronic superposition states are predicted to evolve on suboptical-cycle timescales (3–9). Generating attosecond pulses that can take snapshots of these processes is a prerequisite for understanding electron dynamics that precede, and perhaps even dictate, longer-time nuclear vibrational dynamics. Direct monitoring of electron dynamics necessitates a fundamental technological leap in the generation of ultrashort attosecond pulses, and the next frontier for time-resolved spectroscopy will follow spectroscopic features owing to the motion of electrons on attosecond timescales in real time (10, 11). These experiments have been enabled by the development of methods to generate isolated attosecond pulses from tabletop laser systems, a capability that became available in 2001 (12).

The principle of high harmonic generation (HHG) is at the heart of attosecond pulse production (13–16). This process involves strong-field manipulation of electrons that is facilitated by focusing a femtosecond laser pulse to high intensities in a target material. The target is commonly an inert gas cell held at constant pressure. HHG has also been applied as a tool to study more complex targets, including solids (17–19). The semiclassical picture of HHG generation developed by Corkum (14) follows a three-step model. First, the high field intensities around the maximum of the electric field cycles of the focused driver pulse distort the electronic potential, resulting in tunneling ionization of the gas and the release of electron wave packets into the continuum. Second, the ejected electrons are accelerated away and then toward the parent ion as the laser electric field changes sign, gaining energy from the field. Third, the inelastic recollision of these accelerated electrons with the parent ion releases excess kinetic energy in brief attosecond light bursts when the field cycle approaches a zero crossing. The upper limit for the emitted energy, called the cutoff energy (15, 20), is determined by the maximum amount of kinetic energy gained in the second step and can be expressed as

$$E_{\max} = I_p + 3.17U_p, \tag{1}$$

where I_p is the ionization potential of the target gas, and U_p is the ponderomotive energy of the photoelectrons in the applied electric field, $U_p = E^2_{\text{laser}}/4\omega^2_{\text{laser}}$. Here, E_{laser} is the electric field amplitude of the focused driver pulse, and ω_{laser} is the frequency of the driver pulse. Pulses from Ti:sapphire laser systems centered around 800 nm with peak intensities on the order of 10^{14} to 10^{15} W/cm^2 and pulse durations of a few to hundreds of femtoseconds have been used for single attosecond pulse or pulse train production, resulting in emitted photon energies in the extreme-ultraviolet (XUV) regime. New work uses longer wavelength drivers to achieve higher XUV photon energies (21–25).

If the driver pulse consists of several field cycles, a train of attosecond pulses is generated at different energies in the XUV that interfere with each other, resulting in a high harmonic spectrum that consists of a frequency comb corresponding to multiple recombination events

(26–28). Limiting the number of electric field cycles in the driver pulse reduces the number of recombination events and, consequently, the number of attosecond pulses generated. In conjunction with appropriate energy filtering and carrier-envelope phase stabilization (29) of the driver pulse, few-cycle driver pulses allow for the generation of isolated attosecond pulses without any further optical manipulations (30). In this scenario (called intensity gating), only the most intense half cycle of the driver pulse generates the isolated attosecond pulse, confining the HHG process to the emission of higher XUV photon energies close to the cutoff region. The spectrum of an isolated pulse generated in this way is continuous. Intensity gating has been used to generate pulses as short as 80 as centered at 85 eV (30).

Synthesis of isolated attosecond pulses using longer driver pulses and at lower XUV photon energies that are relevant to core-to-valence state transitions in many interesting systems required the development of other gating techniques. One successful gating technique is polarization gating (31, 32), which exploits the sensitivity of the HHG process to the linear polarization of the driver pulse. The polarization gating technique rests on manipulation of the recollision pathways of the electrons by employing two driver pulses that exhibit counter-rotating elliptical polarization, which are optimally delayed with respect to each other such that only one half cycle of their field oscillations overlaps and creates linear polarization. A central XUV photon energy of 36 eV and a duration of 130 as has been generated with this method (32, 33). Double optical gating imposes an additional constraint to the polarization gating technique by using both the fundamental and second harmonic driver pulses (34–37). This scheme widens the temporal gate width as a result of the broken symmetry from mixing the fundamental and the second harmonic fields, which allows for the use of longer driver pulses for single attosecond pulse generation. Using this method, researchers have generated 67-as pulses (38). Ionization gating is used to confine attosecond pulse generation to the leading edge of an intense driver pulse: Phase matching is destroyed in the gas medium as the rest of the driver pulse propagates, resulting in isolated pulses of ∼430 as (39, 40). Recent work has also utilized wavefront-rotated driver pulses to obtain high harmonic spectra consisting of spatially separated, isolated attosecond pulses (41).

Even though the methodology for producing isolated attosecond pulses is rapidly progressing, technical challenges continue to limit their widespread use in time-resolved experiments. Novel methods such as attosecond angular streaking (or attoclock) (42–45) and core-hole clock spectroscopy (46–48) do not require isolated attosecond pulses. There is also an important and rich literature using attosecond pulse trains to investigate attosecond electronic processes (49–54) (not covered here). Numerous other excellent reviews have also been published on attosecond science over the past few years (10, 11, 33, 45, 55–62). This review focuses on recent scientific insights gained experimentally and theoretically through the use of isolated attosecond pulses and is organized as follows: Section 2 summarizes the major applications of isolated attosecond pulses in time-resolved spectroscopy and their use in studying dynamics in atomic rare gases, Section 3 discusses the scientific advances to study molecules and solids, and Section 4 presents an outlook for future experiments in attosecond science.

2. TIME-RESOLVED SPECTROSCOPY WITH ISOLATED ATTOSECOND PULSES AND THEIR APPLICATION TO ATOMS

Time-resolved spectroscopy is dominated by pump-probe techniques, where a pump pulse creates an excitation in the system under investigation and a probe pulse interrogates this excitation through spectral readout of the pump-induced changes or through photoionization processes. Time evolution is measured by varying the delay between the pump and the probe

FROG CRAB: frequency-resolved optical gating complete reconstruction of attosecond bursts

pulses. Although a true attosecond experiment would involve an attosecond pump pulse and an attosecond probe pulse, the low photon fluxes of existing attosecond sources have precluded such measurements (11). Instead, depending on the system of interest, experiments to date have employed a few-cycle near-infrared or visible femtosecond pulse and an isolated attosecond XUV pulse in various pump-probe pulse sequences. The ability to lock the waveform of the electric field oscillations of the few-cycle pulse allows measurements of dynamics down to subcycle time durations of the femtosecond pulse, thus obtaining attosecond time resolution (63–66). Techniques can use the attosecond XUV pulse as the pump and the few-cycle visible pulse as a probe, and vice versa.

Attosecond time-resolved spectroscopies have been applied in studies of electron dynamics in atoms to address several important questions: How do electrons in an atom respond to an intense optical pulse that imparts a strong oscillating electric field? Can the lifetimes of Auger decay and autoionization be measured directly in real time? How do the valence electrons evolve following strong-field ionization? Furthermore, what states are produced by strong-field ionization, and are they formed in a coherent superposition? Can one determine when a photoelectron is liberated from an atom?

Attosecond pump–few-cycle probe spectroscopies are used extensively in conjunction with ion/electron detection schemes as well as photon detection methods. Attosecond photoelectron streaking is also widely employed as a characterization tool for isolated attosecond pulses (67, 68). This technique uses an attosecond XUV pump pulse to ionize a system, followed in time by a few-cycle visible/near-infrared pulse, a so-called streaking field, that interacts with the emitted electrons. The few-cycle streaking field imparts momentum to the emitted electrons, which is modulated by the oscillating vector potential of the few-cycle pulse at variable time delays. The electron velocity is then mapped by a time-of-flight measurement. The resulting streaking spectrogram, if produced by a direct ionization, tracks the vector potential of the few-cycle field. Upon deconvolution using a FROG CRAB (frequency-resolved optical gating complete reconstruction of attosecond bursts) algorithm (69), it also allows extraction of the duration of the XUV attosecond pulse and the electric field oscillations of the streaking field.

One of the first time-domain experiments using attosecond photoelectron streaking measured the lifetime of the 3*d* core hole in krypton created by an XUV pulse, which is filled by Auger recombination, emitting electrons from the 4*p* shell (70). The emitted electrons interact with a few-cycle near-infrared pulse, and the evolution of the electron kinetic energy from the $M_{4,5}N_1N_{2,3}$ Auger line as a function of the relative delay between the two pulses reveals a 3*d* core hole lifetime of 7.9 fs. This technique has also found extensive use in timing the birth of photoelectrons in atoms (64) and solids (71, 72). An isolated sub-200-as pulse at 106 eV ionizes neon atoms, and the emitted electrons are streaked by a few-cycle near-infrared pulse, resulting in a remarkable delay measured to be 21 ± 5 as in the photoemission of a 2*s* electron relative to a 2*p* electron in neon (64). Multiple theoretical efforts were performed to understand the origin of the measured photoemission delay (73–78) and have thus far underpredicted the observed delay by approximately a factor of two. Possible reasons proposed for this discrepancy include the interaction of the atoms with the streaking field, along with contributions from shake-up satellites and many-electron correlations. Attosecond pump-probe wave-packet interferometry has also been developed, in which an attosecond XUV pulse excites a coherent superposition of bound and continuum states of helium and a delayed near-infrared pulse ionizes the bound states (79). The XUV-created continuum wave packet is used as a reference, and its interference with the continuum wave packet generated from XUV and near-infrared excitation allows for the determination of the composition of the bound electron wave packet, including a 4*p*-5*p* quantum beat.

Attosecond XUV pulses have also been used to initiate an ionization process that is followed in time by a few-cycle near-infrared pulse that doubly ionizes the system under investigation. Ions generated using this pulse sequence are detected by a time-of-flight spectrometer as a function of the time delay between the two pulses, retrieving the electron dynamics of atoms (63) and polyatomic molecules (80, 81). Electron tunneling ionization in neon and xenon is measured in real time using this technique (63). The yield of the doubly ionized Ne^{2+} atoms from tunnel ionization of shake-up electrons, originating primarily from $2p^{-2}4p$, $2p^{-2}3d$, $2p^{-2}3p$, and $2p^{-2}3s$ states, increases in synchrony with the electric field cycles of the near-infrared pulse. For the increase in Ne^{2+} yield, a timescale of 380 as was extracted. A similar experiment in xenon, where Xe^{3+} and Xe^{4+} ions were detected following tunnel ionization from shake-up states, revealed timescales associated with intra-atomic multielectron Auger cascade processes.

Another class of attosecond time-resolved techniques is transient absorption spectroscopy, which measures the spectral response of the sample following interaction with an attosecond XUV pulse and a few-cycle visible/near-infrared pulse (82). This technique is useful to follow dynamics of electrons in bound or autoionizing states. The order in which these pulses interact with the sample determines the information gathered about the system. Pump-probe transient absorption spectroscopies are generally treated in the framework of the third-order polarization in the interaction picture (83, 84), where an intense pulse (usually the pump) represents a second-order interaction and the weaker pulse (usually the probe) represents a first-order interaction, all in the perturbative limit. In near-infrared-XUV attosecond transient absorption spectroscopies, the XUV pulse is much weaker than the near-infrared pulse, regardless of the order in which they interact with the system. Intense few-cycle near-infrared pulses, commonly used in attosecond measurements, impart strong fields to the system and require the inclusion of higher-order response functions. The approach to model these experiments is to first calculate the single atom response (85, 86) and then use various methods to scale this response up to a macroscopic system and include propagation effects (82, 87). This approach treats all nonlinearities in one calculation (85).

The single-atom response is expressed as

$$\tilde{S}(\omega) = -2\mathrm{Im}[\tilde{d}(\omega)\tilde{E}^*(\omega)]. \tag{2}$$

Here, $\tilde{d}(\omega)$ is the Fourier transform of the time-dependent one-electron single-atom dipole moment, and the corresponding macroscopic polarization is $\tilde{P}(\omega) = 2\rho\tilde{d}(\omega)$, where ρ is the density of atoms in the interaction region. $\tilde{E}^*(\omega)$ is the Fourier transform of the electric field. The sign of the single-atom response determines whether light is absorbed (positive) or emitted (negative). The absorption cross section is then written as

$$\sigma(\omega) = 8\pi\alpha\omega\mathrm{Im}\left[\frac{\tilde{d}(\omega)}{\tilde{E}(\omega)}\right], \tag{3}$$

where α is the fine-structure constant.

Transient absorption spectroscopy can be performed with a conventional pulse sequence—near-infrared excitation followed by attosecond XUV probing, where the XUV spectrum is detected after the interaction. This pulse sequence interrogates population dynamics of the system initiated by the near-infrared pump pulse. Using this technique, real-time valence electron motion was resolved in krypton (6), where each cycle of an intense near-infrared pump-pulse strong field ionizes krypton atoms from the $4p$ orbital to generate singly, doubly, and triply charged ions. The attosecond XUV pulse interrogates the excitation through $4p^{-x}$ to $4p^{-x+1}3d^{-1}$ ($1 \leq x \leq 3$) transitions, which are imprinted on the transmitted XUV pulse spectrum. Detailed theoretical analyses (88, 89) reveal that the few-cycle pulse coherently excites the Kr^+ ions to the $4p_{3/2}{}^{-1}$

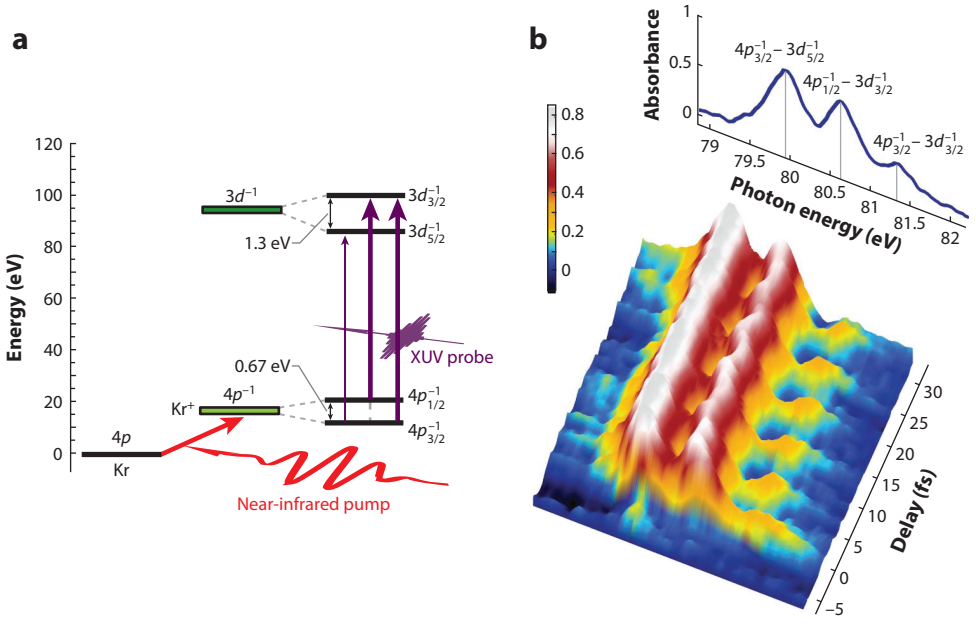

Figure 1

(*a*) Ionization of krypton to Kr^+ via strong-field interaction with the few-cycle near-infrared pump pulse, and subsequent probing from the $4p^{-1}$ to $3d^{-1}$ state of Kr^+ via interaction with an attosecond extreme-ultraviolet (XUV) probe. The $4p^{-1}$ state is spin-orbit split by 0.67 eV into the $4p_{1/2}{}^{-1}$ and $4p_{3/2}{}^{-1}$, which the XUV pulse promotes to the $3d_{3/2}{}^{-1}$ and $3d_{5/2}{}^{-1}$ in the probe step. The coherent superposition formed between these two valence orbital states causes quantum interference in the observed transient XUV spectra shown in panel *b*. (*b*) Pump-probe delay-dependent XUV absorption spectra showing the $4p^{-1}$ to $3d^{-1}$ transitions and their beating in time. Figure reproduced with permission from Reference 6.

and $4p_{1/2}{}^{-1}$ states, launching a spin-orbit wave packet, and the broadband XUV probe pulse projects this population onto the $3d^{-1}$ state. The authors (88, 89) focused on the dipole-allowed transitions of $4p_{3/2}{}^{-1}$–$3d_{3/2}{}^{-1}$, $4p_{1/2}{}^{-1}$–$3d_{3/2}{}^{-1}$, and $4p_{3/2}{}^{-1}$–$3d_{5/2}{}^{-1}$ in Kr^+. As a function of the time delay between the two pulses, a clear quantum interference (quantum beat) is observed for the $4p_{3/2}{}^{-1}$–$3d_{3/2}{}^{-1}$ and $4p_{1/2}{}^{-1}$–$3d_{3/2}{}^{-1}$ transitions with a period of 6.3 $\pm$ 0.1 fs as a result of the modulation in the XUV cross sections as the relative phase of the $4p_{3/2}{}^{-1}$ and $4p_{1/2}{}^{-1}$ states evolved (**Figure 1**). The time-dependent phase information is understood as a time-dependent hole density distribution of the $4p$ state in Kr^+, which shows dramatic modulation through valence hole alignment on a few-femtosecond timescale. Numerical modeling and comparison with experimental data allowed a complete characterization of the reduced-density matrix of Kr^+.

Several studies of rare gases have used a less intuitive pulse sequence in which the XUV pulse precedes the near-infrared pulse. This method has been used to unravel quantum pathways and electron dynamics (82). Owing to the long dephasing times of the sharp atomic resonances, the macroscopic oscillating dipole induced by the XUV pulse is perturbed by a delayed near-infrared pulse, thus modifying the XUV spectral lineshape on timescales as long as a few femtoseconds or more. This process (illustrated in **Figure 2**) is akin to perturbed free-induction decay measurements (83), with the exception that the near-infrared pulse is ultrashort and intense. This method has been successfully applied to many rare gas systems, where the coupling of electronic states with the near-infrared pulse reveals new spectral features corresponding to light-induced states (90, 91)

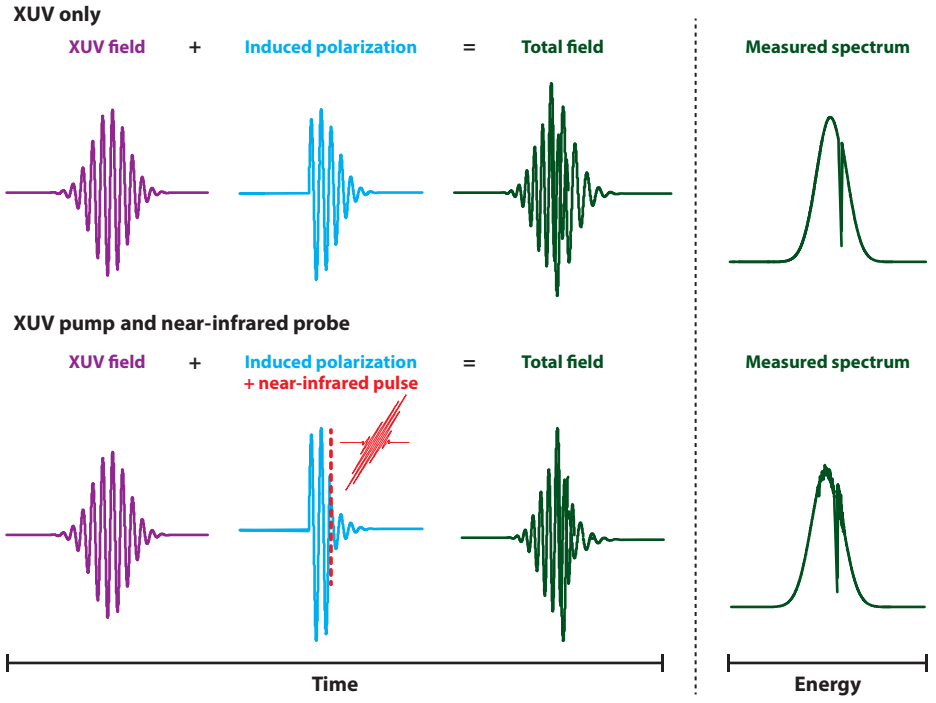

Figure 2

Illustration of an extreme-ultraviolet (XUV) pump–near-infrared probe experiment. In the presence of the XUV pulse alone (*top*), the time behavior of the induced macroscopic polarization provides the XUV spectrum of the system. The addition of a near-infrared pulse after the XUV-pulse interaction (*bottom*) perturbs the temporal behavior of the induced polarization, resulting in modifications to the XUV spectrum that can be related to dynamic properties of the system.

and Autler-Townes splitting (87, 92). Theoretical efforts have been crucial to understanding the intense few-cycle pulse interaction with atoms and the resulting quantum pathways that underlie the spectral features measured by an attosecond XUV pulse (7, 86, 93, 94). The near-infrared pulses in these experiments also cause a phase shift in the induced dipole moment, resulting in changes to the lineshape of the transmitted XUV spectrum from Lorentzian to Fano (9, 95).

Time-dependent measurements with pulse sequence XUV first, time-delayed near-infrared pulse second have been used to characterize the lifetimes of autoionizing states in rare gas atoms, where the population is depleted in the initially excited state by coupling to the ionization continuum or in other states by the near-infrared pulse as a function of the pump-probe delay. This depletion recovers as the near-infrared pulse is delayed in time after the XUV pulse, and the timescale for this recovery is related to twice the lifetime of the autoionizing state. This technique has been applied in studies of autoionizing states in argon where the $3s3p^6np$ transitions exhibit a shift, broadening and weakening, and the $3s3p^64p$ and $3s3p^65p$ lines recover with lifetimes of 8.2 fs and 23.3 fs, respectively, in agreement with frequency-domain measurements of the line widths (96). A similar experiment was performed on xenon (94), yielding autoionizing lifetimes of the $5s5p^66p$ and $5s5p^67p$ states equal to 21.9 $\pm$ 1.3 fs and 48.4 $\pm$ 5 fs, respectively. Quantum beats from XUV excitation of multiple electronic states in neon are also observed, where the $2s^22p^5(^2P_{1/2})3d$ and $2s^22p^5(^2P_{3/2})3d$ states exhibit a beat period of 40 fs (9). Similar methods have

been applied to argon and to small molecules such as H_2, where individual vibrational states are also measured (97).

3. ULTRAFAST CHARGE MIGRATION IN MOLECULES USING ATTOSECOND PULSES

3.1. Ultrafast Charge Localization in Small Molecules

Investigations of attosecond electron dynamics in atoms have been extended to studies of charge redistribution in small molecules on subfemtosecond timescales to explore the coupling between electronic and nuclear degrees of freedom in the non-Born-Oppenheimer regime. By comparing the intensities of the high harmonics between the two isotopes, Marangos and coworkers (98) used the HHG process as a pump-probe (ionization-recollision) technique in H_2 and D_2 and in CH_4 and CD_4 to determine the dynamics of nuclear wave-packet motion of the molecular ion with a 100-as resolution. This approach measures the change in the symmetry of the CH_4 molecule from tetrahedral geometry to planar C_{2v} geometry upon ionization, which occurs on a few-femtosecond timescale. Earlier work by Kling et al. (99) studied dissociative ionization of D_2 using an intense waveform-controlled few-cycle near-infrared pulse: By changing the phase of the electric field of the few-cycle pulse, the authors demonstrated subfemtosecond control over the localization of the electron on either of the two atoms in D_2. A recent experiment using isolated attosecond pulses was performed to follow charge localization in the hydrogen molecule upon dissociative ionization (80). This study measured the ultrafast charge redistribution in hydrogen and deuterium molecules following dissociative ionization to explore the coupling between electronic and nuclear motion on subfemtosecond timescales. Here, the pulse sequence consisted of an isolated attosecond XUV pulse ranging from 20 to 40 eV that excites the molecule to higher-lying electronic states followed by an intense 6-fs, full width at half maximum (FWHM) few-cycle near-infrared pulse that couples this excitation to nearby states. The velocity and angular distributions of the resulting H^+ or D^+ photofragments are analyzed as a function of the delay between the two pulses.

An asymmetry parameter is defined to understand the observed time-dependent evolution of the photofragments and electrons emitted in different directions. Two types of asymmetries are considered—a laboratory-frame asymmetry due to the asymmetry in the fragment ejection about the polarization axis and a molecular-frame asymmetry caused by asymmetry of the electron and ion ejections from the molecule. As the time delay between the two pulses is varied, a pronounced oscillation of the asymmetry is observed at all detected kinetic energies of the D^+ or H^+ ion fragments on a suboptical cycle timescale.

One mechanism (shown in **Figure 3**) for asymmetry oscillation is explained as originating from the interference of electron wave packets launched by XUV-only or XUV and near-infrared excitations during temporal overlap. The second mechanism is described as a process where the near-infrared pulse modifies the wave function of the molecular ion during dissociation, after the photoexcitation process. In this mechanism, the intense near-infrared pulse transfers population between the $1s\sigma_g$ and the $2p\sigma_u$ states following the XUV-initiated electronic excitation of the molecule to the $2p\sigma_u$ state. Because the degree of population transfer varies as the molecule traverses these states along the nuclear coordinate, R, this explanation is supported using a Landau-Zener model for a two-level system consisting of the $1s\sigma_g$ and the $2p\sigma_u$ states, with an R-dependent energy splitting. At the end of the dissociation process, the electron settles in localized superposition states. This work is seminal in using attosecond spectroscopy to understand how coupling with nuclear motion dictates localization of the electronic distribution in a diatomic molecule on suboptical-cycle timescales.

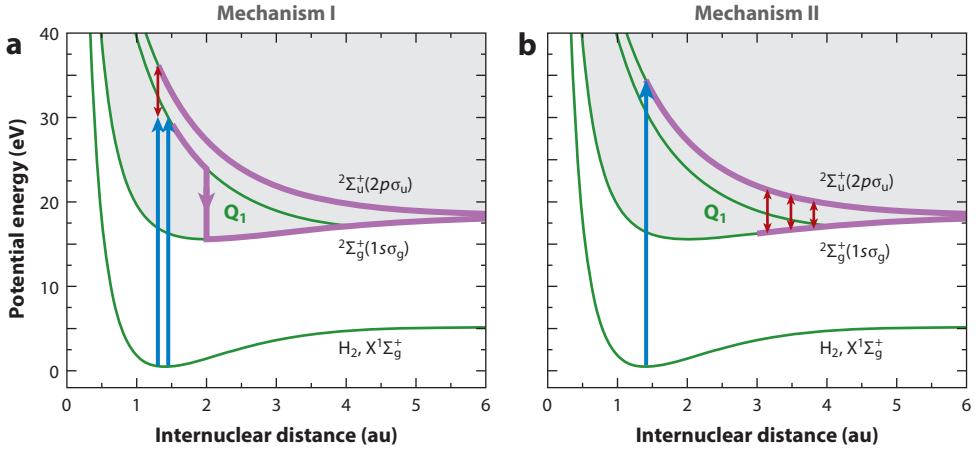

Figure 3

Two proposed mechanisms for an extreme-ultraviolet (XUV) and near-infrared interaction with the hydrogen molecule: (*red arrows*) near-infrared pulse, (*blue arrows*) XUV pulse. Mechanism I (*left*) shows the interaction of the two pulses when temporally overlapped during photoexcitation, and Mechanism II (*right*) displays the interaction at longer delays between the XUV and near-infrared pulses during dissociation. Figure reproduced with permission from Reference 80.

3.2. Theoretical Investigations of Ultrafast Charge Migration in Polyatomic Molecules

Experimental work by Schlag, Weinkauf, and coworkers in the 1990s (100–102) suggested that through-bond charge migration in peptides occurs after localized ionization, as evidenced by nonstatistical dissociation channels. These experiments motivated theoretical work that has led to a new subfield in attosecond science. Attosecond investigations in large molecules may lead to an understanding of the role of correlation-driven electronic redistribution in molecules on sub- to few-femtosecond timescales, preceding slower electron transfer dynamics mediated by coupling to nuclear coordinates (103). This is at the core of so-called post-Born-Oppenheimer dynamics (5). Cederbaum and coworkers (104–111) and Levine and coworkers (4, 5, 102, 112–116) performed extensive theoretical calculations that model charge migration processes in various polyatomic molecules.

In 1999, Cederbaum & Zobeley (103) proposed that a localized hole could redistribute across a molecule purely as a result of electron correlation effects on a timescale of a few femtoseconds, before the onset of nuclear motion. The theory considers the migration of charge density in molecules with frozen nuclear coordinates following ultrafast ionization, assuming that the initially created hole originates from a localized orbital creating a nonstationary state that evolves with time. In the absence of many-body electron interactions, the charge density would simply remain in the initial state. The presence of many-body electron correlation effects causes the hole charge density to redistribute within the molecule.

The hole charge density at location $\mathbf{r}$ and time t has been defined as (106)

$$Q(\mathbf{r}, t) = \langle \Psi_0 | \hat{\rho}(\mathbf{r}, t) | \Psi_0 \rangle - \langle \Phi_i | \hat{\rho}(\mathbf{r}, t) | \Phi_i \rangle, \quad (4)$$

where Ψ_0 is the ground-state wave function of the system, Φ_i is the nonstationary state created after ionization, and $\hat{\rho}(\mathbf{r}, t)$ is the charge density operator. The first term is time independent, whereas the second term describes the time-dependent evolution of the charge density.

The spatially resolved time-evolving charge density is expressed as

$$Q(\mathbf{r}, t) = \sum_i \omega_i(t)|\varphi_i(\mathbf{r}, t)|^2, \quad (5)$$

HOMO: highest occupied molecular orbital

where $\omega_i(t)$ is the occupation number of the time-dependent hole orbital denoted by $\varphi_i(\mathbf{r}, t)$. The hole density is computed using ab initio methods. A sudden approximation is applied in the calculations, where it is assumed that the hole is created by abrupt ionization, on timescales shorter than the migration of charge within the molecule (106). Such sudden ionization in molecules has been achieved experimentally using attosecond pulses (see Section 3.3).

This principle has been applied to model charge migration in numerous polyatomic molecules, where the initial ionization is from either the outer- or inner-valence orbitals. Two major mechanisms by which charge migrates have been identified: a hole-mixing mechanism arising from superpositions of one-hole cationic states predominant for outer-valence ionization, and a dominant satellite mechanism due to the presence of two-hole–one-particle satellite peaks around a main one-hole state, which is predominant for inner-valence ionization (110). The methodology shows that, in a system such as *para*-cresol (HO-C_6H_4-CH_3) (106), an initially created hole residing in an inner-valence orbital on the methyl group traverses across the aromatic ring to the hydroxyl group in less than 2 fs. The hole then oscillates back to the methyl group with a period of 2 fs, without significant charge density detected on the aromatic ring. This methodology was also applied to understand outer-valence shell ionization in the polyatomic molecule 2-phenylethyl-*N*, *N*-dimethylamine, another experimentally studied system (117), where three hole orbitals contribute to the charge migration—one at the nitrogen site and two from π-orbitals of the benzene ring (105). In this case, an initially created hole on the benzene ring migrates to the nitrogen site in less than 4 fs via the hole-mixing mechanism. Similar calculations have been performed on other molecules, thus showing a dependency of the mechanism of ultrafast charge migration on molecular conformation (104), symmetry (109), and substitutions (8).

Cederbaum (104, 109), Levine (4, 113), and their coworkers investigated the dependence of charge migration in amino acids and peptides on the orbital from which the initial ionization happens. Kuleff et al. (118) showed that ionization from inner- and outer-valence orbitals of glycine results in different charge migration dynamics. Ionization from an inner-valence orbital located on the CO and OH groups of glycine distributes over the entire molecule in ∼8 fs through hole mixing and dominant satellite mechanisms. By contrast, ionization from an outer-valence orbital located on the NH_2 group migrates to the CO and OH end of the molecule in 3.5 fs via a hole-mixing mechanism. Levine and coworkers (4, 113) also investigated charge migration in small tetrapeptides. The authors computed time-evolving hole charge densities in singly ionized tetrapeptides at the equilibrium nuclear geometries of the neutral molecules. The tetrapeptides studied were $Trp(Leu)_3$, $Trp(Ala)_3$, and $Tyr(Ala)_3$, and calculations were performed for ionization from different molecular orbitals to assess the differences in the timescales for charge migration. As a result of ionization of $Trp(Leu)_3$ from the delocalized π-like highest occupied molecular orbital (HOMO), the hole density is created on the Trp end and migrates to the N terminus by 750 as and back to the Trp end by 1.5 fs. By contrast, owing to ionization of $Trp(Ala)_3$ from a deeper localized σ-like molecular orbital, the hole density remains in the Trp end on a 1-fs timescale.

Remacle & Levine (119) studied charge migration in hydrogen-bonded dimers to explore the differences in initial hole localization and redistribution based on the symmetry of the dimer. They considered the asymmetric water-water and methanol-water dimers as well as the symmetric NO-NO dimer. In the water-water dimer, the HOMO of the neutral dimer was localized on one of the water molecules and was a superposition of two molecular orbitals, the HOMO and the lowest

unoccupied molecular orbital (LUMO), of the cation. A hole created on one water molecule by ionizing from the HOMO of the neutral dimer migrated to the other molecule and back with a periodicity of 4.13 fs.

LUMO: lowest unoccupied molecular orbital

Dutoi et al. (107) computed the correlated hole and particle mobilities in molecules and found that the timescales over which the electrons and holes migrate depend on whether substituted atoms add or remove electrons from the system. Recent work extends these calculations to predict attosecond XUV transient absorption of polyatomic molecules (111, 120). Calculations of a few-femtosecond pump and attosecond XUV probe ultrafast ionization have also been conducted to study charge migration in a polyatomic molecule (116).

3.3. Ultrafast Electron Dynamics in Phenylalanine

Theoretical investigations of ultrafast charge migration in large molecules spawned experimental efforts to study the migration of charge density following rapid attosecond photoionization of polyatomic systems. Recently, Calegari et al. (81) used isolated attosecond pulses to perform such measurements in the amino acid phenylalanine in the gas phase. Here, a single sub-300-as pulse ranging in energy from 15 to 35 eV is employed as the pump pulse to cause sudden ionization of phenylalanine. An optical waveform-controlled 4-fs probe pulse then ionizes the molecule a second time, resulting in the dissociation of the -COOH fragment from the parent molecule. The doubly charged immonium fragments ($R\text{-}CH\text{-}NH_2^{2+}$) left behind after the dissociation are detected using a time-of-flight mass spectrometer as a function of the time delay between pump and probe pulses. Experiments using a different XUV spectrum with a width of 3 eV and centered at 15 eV found that the immonium yield is negligible because the lower XUV energy requires the absorption of more visible/near-infrared photons for dication formation, suggesting that the dications are born from highly excited states of the singly charged cation. Because molecular conformation can dictate charge migration dynamics, the authors calculated that only 6 of the 37 conformers of phenylalanine at the experimental temperature of 430 K are important.

Important dynamics are measured at very early time delays, where the immonium fragment yield oscillates with an average period of 4.3 fs (see **Figure 4*a***). Calegari et al. (81) performed Fourier analysis of the frequency components of the oscillation at all the pump-probe time delays. At short delays of less than 15 fs, the oscillations exhibit two strong frequency components at 0.14 PHz and 0.3 PHz, which decay and give rise to a component at 0.24 PHz for time delays between 15 fs and 35 fs. Because the highest vibrational frequency associated with the X-H stretching modes in phenylalanine is 0.11 PHz, lower than the frequencies extracted from the experimental data, the authors indicate that the periodicity observed may be due to electronic effects that are only partly influenced by nuclear motion.

Theoretical calculations of the hole density were performed from the time of ionization by the XUV pulse to 500 fs using time-dependent first-order perturbation theory and time-dependent density matrix formalism for a system described by a sum of single-particle Hamiltonians of one-hole cationic states. After performing orientational averaging, recurrences with a 3–4-fs periodicity are observed for hole densities localized on the amine group (see **Figure 4*b***), in agreement with the experimental observation of beating in the immonium photofragment yield. Fourier analysis of these calculations reveals frequency components similar to those seen in experiments. However, the intensities were not in agreement, presumably as a result of neglect of the probe-pulse interaction with the system in the calculations. Despite qualitative agreement, the authors (81) did not exclude the possibility that nuclear dynamics play a role in the charge density recurrences. As they noted, charge density beating is observed following the creation of a delocalized initial state owing to the superposition of many one-hole cationic states. This important work shows for the

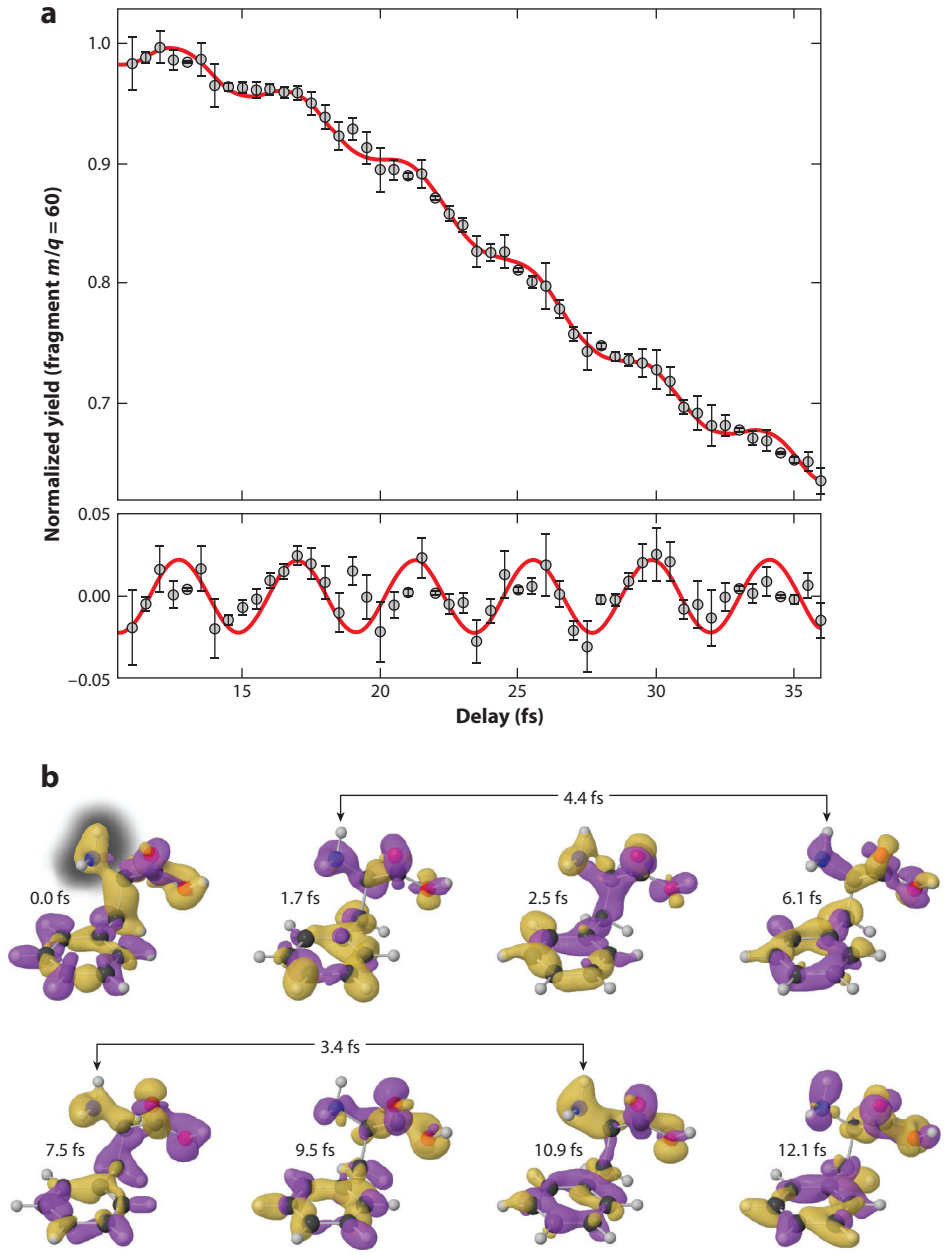

Figure 4

(*a*) Immonium dication photofragment yield as a function of extreme ultraviolet pump–near-infrared probe delay. Experimental data are displayed as black dots, and the sum of an exponential curve and a sinusoidal oscillation with 0.234-PHz frequency is displayed in red. The sinusoidal oscillation alone is shown in the lower panel. (*b*) Calculated changes to the hole density distributions across the most abundant conformer of the immonium fragment, showing oscillations in the hole density at the amine group on a few-femtosecond timescale. Figure reproduced with permission from Reference 81.

first time that broadband attosecond XUV ionization can elicit modification of the overall charge density and recurrences within a large molecule on subfemtosecond timescales.

4. ATTOSECOND ELECTRON DYNAMICS IN THE CONDENSED PHASE

Time resolution of the motion of electrons in solids is the goal of several recent attosecond investigations. Researchers have employed both photoelectron and transient absorption spectroscopies to consider questions associated with electron transport in metals (71, 72, 121, 122), electron interactions in semiconductors (66), and fast switching of conductivity in dielectrics (65). Complications exist with both techniques: Owing to the low escape depth of electrons, photoelectron spectroscopy can probe only near-surface dynamics, and it requires a very clean sample surface under ultrahigh vacuum conditions. Transient absorption spectroscopy requires very thin samples on the order of tens to hundreds of nanometers owing to short attenuation lengths and to avoid temporal deviation between the pump and probe pulses as they travel through the sample, which would otherwise jeopardize time resolution. Despite these challenges, many interesting questions pertaining to the behavior of electrons in solids can be addressed with attosecond spectroscopy: What determines the escape time of electrons from metal surfaces? What are the timescales that govern electron-electron and electron-phonon interactions in semiconductors? Can a large band-gap dielectric be turned into a conductor, and if so, how rapid is this transformation? Theoretical efforts also propose applying attosecond techniques to understand electron dynamics responsible for the rise and decay of plasmon resonances in nanoparticles (123–125).

4.1. Surface Electron Dynamics in Solids Probed by Attosecond Photoelectron Streaking

In an attempt to follow the transport of electrons to a solid surface in real time, attosecond photoelectron streaking spectroscopy was applied for the first time to study dynamics of electron escape from core and delocalized electronic states of a single crystalline tungsten <110> surface (71). The experiment employed isolated XUV pulses with a pulse duration of ~300 as centered at 91 eV with a 6-eV FWHM to simultaneously excite the 4*f* core level and the 5*d* and 6*s* conduction band electrons to upper conduction band states of tungsten, leading to the creation of photoelectrons at the surface. The photoelectrons exhibit kinetic energy, $KE_{\mathrm{elec}} = E_{\mathrm{XUV}} - E_{\mathrm{bind}} - \phi$, where E_{XUV} is the energy of the incident XUV pulse, E_{bind} is the binding energy of the electron, and ϕ is the work function of the material. A few-cycle waveform-controlled ~5-fs near-infrared pulse at 750 nm is used to streak (momentum shift) the emitted photoelectrons. The measured spectrogram consists of two photoelectron peaks centered at kinetic energies of 56 eV from the 4*f* photoelectrons and 83 eV for the photoelectrons emerging from the conduction band states, both of which are successfully streaked by the vector potential of the streaking laser pulse. The resulting attosecond streaking spectrogram, following numerical corrections to above-threshold ionization background from multiphoton near-infrared absorption, revealed a delay of 110 ± 70 as in the emergence of 4*f* electrons relative to the conduction band electrons from the tungsten surface.

The origin of this delayed photoemission is explained by differences in the transport of 4*f* and conduction band electrons to the surface. The results were analyzed based on variations in the group velocity of the photoelectrons emerging from the 4*f* and conduction band levels. The 4*f* electrons, which are slower than the conduction band electrons and characterized by a longer inelastic mean free path, originate 1 Å deeper in the material than do the conduction band electrons. The absolute delays between the photoionization pulse and the emergence of photoelectrons for the conduction band and 4*f* electrons were ~60 as and ~150 as, respectively (71).

This experiment spurred theoretical investigations of the phenomenon, which reproduced the measured delay but proposed contradictory interpretations for its origin. Semiclassical calculations, where Langevin dynamics were used to describe classical electron transport with stochastic collisional momentum transfer treated with quantum scattering, suggested that the delay was due to electron propagation effects (126). Further quantum mechanical calculations (127) have supported the experimental conclusion that the delay was from propagation effects, but they added that the interference between photoelectrons emerging from the 4*f* orbital from different layers of the solid contributed more significantly. However, time-dependent fully quantum mechanical calculations (128, 129) have indicated that the delay arises as a result of differences in the localization of the 4*f* and conduction band electronic states, where the localized relatively strongly bound 4*f* electrons escape later than do the delocalized conduction band electrons.

A follow-up experiment was performed in magnesium, a free-electron metal, to establish if the delay in the photoemission from a metallic surface was due primarily to electron transport or if the nature of the initial states of the electrons played a role (72). Magnesium was chosen owing to its efficient screening of the near-infrared field at the surface, avoiding field penetration into the material. This work also reported that the conduction-band states of magnesium are significantly more delocalized than are the 2*p* core level states, providing a greater contrast than the 4*f* and conduction band states of tungsten. Within experimental error, this measurement revealed no measurable time delay between the photoemission from 2*p* (kinetic energy of ~68 eV) and conduction band states (kinetic energy of 115 eV) of magnesium. This observation was justified as an offsetting effect between the longer mean free path (5.9 Å) of the higher–kinetic energy conduction band electrons and a shorter mean free path (4.8 Å) of the lower–kinetic energy 2*p* electrons at 68 eV. On the basis of a quantum mechanical model, photoemission of electrons from these states was estimated to occur coincidentally at 92 as following excitation, with no discernable relative delay. The results lend further credence to the interpretation of the delay in tungsten as originating from electron propagation effects through the metal as opposed to the different degrees of localization of the initial electronic states (72, 130).

4.2. Attosecond Field-Induced Tunneling of Electrons in Silicon Dioxide

Attosecond transient absorption spectroscopy has been added to the toolbox to study solid-state systems and has been successfully applied to investigate electron dynamics in bulk solids. The first such experiment was performed in the dielectric material silicon dioxide, where an intense waveform-controlled <4-fs few-cycle pulse with a carrier wavelength of 780 nm excites the material and a 72-as XUV pulse probes changes induced by the excitation on the *L*-edge (2*p*-to-conduction band) absorption of silicon (65). The SiO_2 studied in these experiments is a 125-nm-thick free-standing sample, and the band gap is ~9 eV. The experiment showed a >10% instantaneous change in the *L*-edge absorption of silicon across the energy range of the conduction band accessed by the XUV pulse, which occurs at twice the frequency of the near-infrared field oscillations (**Figure 5**). Attosecond photoelectron streaking from a neon target was used to characterize the electric field oscillations of the near-infrared pump pulse (**Figure 5*b***), and the field strength at the peak of the pulse was quantified as 2.5 ± 0.5 V/Å. Changes to the *L*-edge absorption manifest as both transient reduction in the sample absorption from 109 eV to 120 eV and a transient red shift in the position of the onset of the conduction band absorption around 109 eV. These *L*-edge modifications occur only in the presence of the near-infrared excitation and are fully reversible after the passage of the excitation pulse.

Theoretical calculations that numerically and nonperturbatively solve the time-dependent Schrodinger's equation in the presence of a strong-field laser pulse in combination with Maxwell's

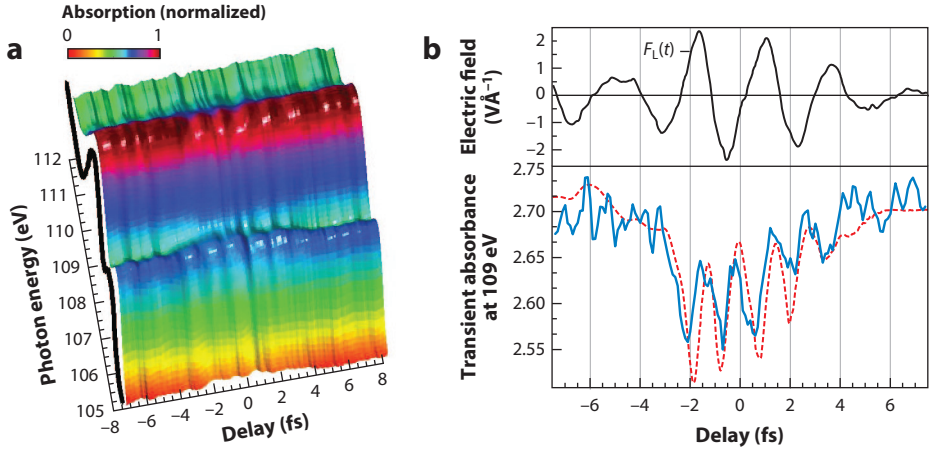

Figure 5

(*a*) Attosecond transient absorption spectrogram of the *L*-edge of SiO_2 as a function of delay between the near-infrared pump and extreme-ultraviolet (XUV) probe pulses and the XUV photon energy. Oscillations induced by the near-infrared electric field are clearly visible. (*b*) Electric field oscillations of the near-infrared pump pulse (*top*, *black*) extracted from a streaking measurement, the transient absorption signal at 109 eV (*blue*) as compared with the theoretically calculated transient absorption (*dashed red*), showing oscillations at every extremum of the near-infrared electric field. Figure reproduced with permission from Reference 65.

equations were used to interpret the experimental results. The results from the calculations agreed with the measured phase, amplitude, and the nature of the instantaneous field-induced oscillations of the *L*-edge transition onset at 109 eV following near-infrared excitation of SiO_2. These calculations reveal that the induced polarization in the material follows the instantaneous electric field of the optical excitation pulse and, hence, is also fully reversible. The transient red shift in the conduction band onset is identified as a dynamic Stark shift. The theoretical estimate for the percentage of conduction band population is ~6% at the peak of the field oscillations for intensities right below the material damage threshold. In the model, light-field-induced transient changes to the conduction band population are responsible for the reversible and instantaneous changes observed in the transient XUV absorption. This increase in conduction band population is supported by near-infrared pump–near-infrared probe reflectivity measurements that show an increase in reflectivity due to metallic conductivity when the two pulses are overlapped.

These results were described using the Wannier-Stark ladder. The transient increase in the polarizability resulting in dynamic Stark shifts of the bands causes the increase in the conduction band population by bringing the states into resonance with the near-infrared excitation pulse. These spectroscopic measurements were later supported by experiments that measured transient electric currents in SiO_2 that were manipulated on a subfemtosecond timescale using a few-cycle waveform-controlled near-infrared pulse (131). This work, afforded by the attosecond time resolution and intense light field interaction, showed for the first time that an insulator can be turned into a conductor and back on subfemtosecond timescales driven purely by the electronic response of the material in the presence of the strong field.

4.3. Attosecond Band-Gap Dynamics in Silicon

Attosecond transient absorption experiments have been extended to a semiconductor to investigate the electron dynamics during and immediately following band-gap excitation. The system studied

is bulk single crystalline silicon. Unlike in the wide-gap dielectric SiO_2, the band structure of silicon accommodates an indirect 1.1-eV band gap and a direct 3.2-eV band gap. A waveform-controlled intense few-cycle near-infrared excitation pulse of <5 fs centered at 760 nm is used to excite silicon primarily across the direct gap. Then, an XUV pulse of <100-as duration centered at ~100 eV is used to probe the *L*-edge (2*p*-to-conduction band) transition of silicon. Experimental results were corroborated by ab initio time-dependent density functional theory (TD-DFT) calculations (132) that model the interaction of an intense laser pulse with silicon and by core-level absorption calculations (133) that translate the output from the ab initio calculations to *L*-edge absorption spectra for comparison with experimental results.

The *L*-edge absorption of silicon shows a sharp onset at ~100 eV, reflecting the conduction band minimum, with rich substructure features above the onset. Excitation across the relatively modest band gap of silicon resulted in a lasting change to the transient *L*-edge absorption, indicating the transfer of population from the valence to the conduction band that survives the duration of the near-infrared pulse. TD-DFT calculations using similar excitation-pulse properties as those used in the experiment suggested that the band-gap excitation is in the tunneling regime where the strong laser field causes the conduction and valence bands to bend and the electrons tunnel across the band gap, thus leading to a nonequilibrium distribution of carrier population in the conduction band. This excitation can approximately be described as an ionization because the valence band is made of orbitals in the bonded regions of the silicon lattice, whereas the conduction band is delocalized in the interstitial regions (134). All the excitation energy is supplied in an ultrashort burst, resulting in an excitation that is dependent on the electric field amplitude as opposed to the intensity required in conventional ionization processes with longer pulses or continuous-wave sources (135).

Changes to the *L*-edge absorption (displayed in **Figure 6*a***) manifest as broadening of the substructures and enhanced absorption below the unperturbed conduction band onset, both surviving the duration of the near-infrared pulse. The substructure broadening, which is the dominant change observed, is interpreted in the time domain as a faster dampening of the XUV dipolar oscillations caused by carrier-carrier interactions in the conduction band. The changes to the *L*-edge follow twice the frequency of the near-infrared field, leading to subcycle oscillations

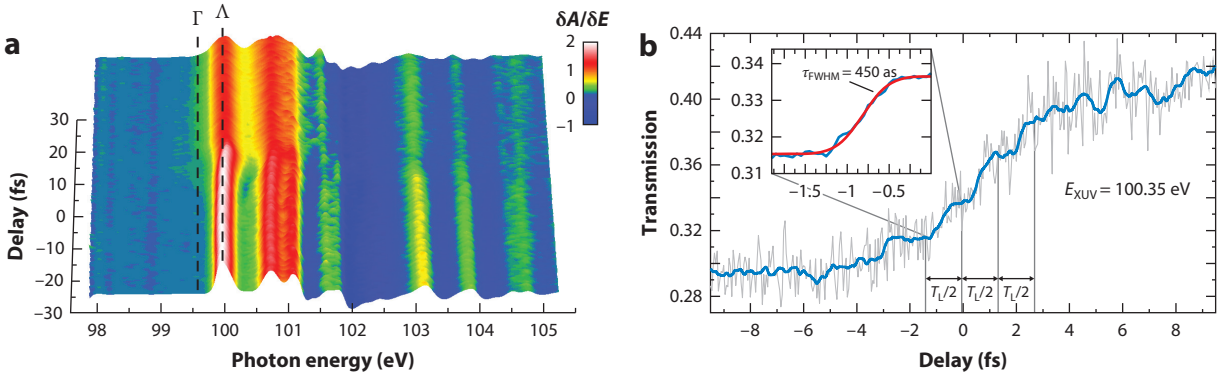

Figure 6

(*a*) Derivative of the *L*-edge absorption of silicon showing the enhanced absorption below the *L*-edge onset (conduction band minimum) denoted by Γ and transient field-induced blue shift denoted by Λ. The peaks also exhibit a broadening as the time delay changes from negative to positive. (*b*) Synchronized subcycle oscillations of the *L*-edge transmission at 100.35 eV at twice the carrier frequency ($1/T_L$) of the near-infrared pump pulse. The inset shows a 450-as rise time of these oscillations. Abbreviations: FWHM, full width at half maximum; XUV, extreme ultraviolet. Figure reproduced with permission from Reference 66.

of the measured XUV absorption as a function of pump-probe time delay (**Figure 6*b***). Thus, with every extremum of the field oscillation, electrons are transferred to the conduction band, and the underlying carrier-carrier interaction occurs faster than the half-cycle period of the driving laser pulse. Fitting each subcycle oscillation with an error function yields a timescale of ~450 as, indicating a possible timescale for carrier-carrier interaction in highly excited silicon.

A persistent shift of the conduction band onset of 121 meV was observed (see **Figure 6*a***), which is attributed to both the core-level shift due to the conduction band population and the downshift of the conduction band minimum due to band-gap narrowing. Band-gap narrowing has been observed universally in static transmission measurements of many doped semiconductors (136). These measurements attribute the initial narrowing to a purely electronic process. In conjunction with theory, the observed band-gap narrowing is ascribed to a carrier density of $\sim 10^{21}$ electrons/cm^3 promoted by the near-infrared pulse.

These experiments reveal that attosecond transient absorption spectroscopy can be used to follow electron dynamics in semiconductors. In conjunction with state-of-the-art theoretical calculations, it may also provide significant insight into relevant processes such as electron-electron and electron-lattice interactions as well as real-time resolution of the tunneling mechanism governing few-cycle band-gap excitation.

5. OUTLOOK

More than a decade after the generation of isolated attosecond XUV pulses, various types of attosecond spectroscopy have been developed and applied to time-resolving electron dynamics in a variety of systems ranging from noble gas atoms and polyatomic molecules to metallic, dielectric, and semiconducting materials. The next frontier in the application of this technology lies in extending these studies to explore more complex gas-phase and solid-state phenomena, primarily driven by strong electron correlation effects. Attosecond spectroscopy can be applied to studies of nonadiabatic dynamics across conical intersections where nuclear and electronic degrees of freedom are strongly coupled and can evolve on a few-femtosecond timescale. These studies will extend investigations of electron dynamics in systems supporting a breakdown of the Born-Oppenheimer approximation (137). Exciting multiple electronic states in a molecule using broadband attosecond XUV pulses may reveal interesting dynamics due to quantum interferences from which lifetimes of short-lived states can be determined. Further application of attosecond spectroscopy to explore charge migration processes in polyatomic molecules will open doors to understanding the role of chemical structures and compositions in ultrafast electronic charge redistribution that precedes nuclear dynamics.

In the condensed phase, attosecond transient absorption and streaking spectroscopies above and below transition temperatures of strongly correlated systems such as materials that exhibit a metal-to-insulator transition and superconductors may help reveal the role of many-electron correlations on the dynamics that underlie these phase transitions (138–141). Extending attosecond studies to more complex semiconductors and nanostructures may shed light on dynamics associated with exciton formation, dissociation, and transport. Generation of attosecond pulses at higher photon energies will allow exploration of carbon-based materials such as organic photovoltaics via attosecond probing of the carbon *K*-edge. Attosecond photoelectron streaking may also reveal many-electron plasmonic motion in metallic nanoparticles, as has been theoretically proposed (123–125).

To date, attosecond experiments have involved strong-field interaction with a few-cycle laser pulse and a perturbative interaction with an attosecond XUV pulse. Understanding results from these experiments is nontrivial and often requires high-level theoretical calculations to model

strong-field light-matter interactions that significantly affect the electronic states of the system. Technical improvements involving generation of intense attosecond pulses and sophisticated detection techniques will allow for the development of true attosecond pump-probe experiments where dynamics are observed after perturbative interactions with attosecond XUV pump and probe pulses (142) as well as two-color experiments that involve single-photon interactions with a visible or near-infrared pulse and an attosecond pulse. These studies can be aided by theoretical calculations in the perturbative limit. Improving attosecond XUV sources will allow for the generation of multiple attosecond pulses of sufficient intensity that can be used in multidimensional spectroscopy, similar to what is performed in the visible and infrared regimes, where electronic correlations and coherences can be measured with the ability to disentangle broad electronic transitions typical in solids (143).

DISCLOSURE STATEMENT

The authors are not aware of any affiliations, memberships, funding, or financial holdings that might be perceived as affecting the objectivity of this review.

ACKNOWLEDGMENTS

This research has been supported by the Director, Office of Science, Office of Basic Energy Sciences, of the US Department of Energy under contract DE-AC02-05CH11231, the Wm. H. Keck Foundation, the Defense Advanced Research Projects Agency PULSE program through grant W31P4Q-13-1-0017, and the Multidisciplinary University Research Initiatives from the Army Research Office (WN911NF-14-1-0383) and the Air Force Office of Scientific Research (FA9550-15-1-0037). S.R.L. acknowledges support from a National Security Science and Engineering Faculty Fellowship (NSSEFF) and from the National Science Foundation under grant CHE-1361226. K.R. acknowledges support from an NSSEFF grant.

LITERATURE CITED

1. Khundkar LR, Zewail AH. 1990. Ultrafast molecular reaction dynamics in real-time: progress over a decade. *Annu. Rev. Phys. Chem.* 41:15–60
2. Ashcroft NW, Mermin ND. 1976. *Solid State Physics.* Philadelphia, PA: Saunders
3. Schweigert I, Mukamel S. 2007. Coherent ultrafast core-hole correlation spectroscopy: X-ray analogues of multidimensional NMR. *Phys. Rev. Lett.* 99:163001
4. Remacle F, Levine RD. 2007. Probing ultrafast purely electronic charge migration in small peptides. *Z. Phys. Chem.* 221:647–61
5. Muskatel BH, Remacle F, Levine RD. 2009. The post-Born-Oppenheimer regime: dynamics of electronic motion in molecules by attosecond few-cycle spectroscopy. *Phys. Scr.* 80:048101
6. Goulielmakis E, Loh Z-H, Wirth A, Santra R, Rohringer N, et al. 2010. Real-time observation of valence electron motion. *Nature* 466:739–43
7. Santra R, Yakovlev VS, Pfeifer T, Loh Z-H. 2011. Theory of attosecond transient absorption spectroscopy of strong-field-generated ions. *Phys. Rev. A* 83:033405
8. Dutoi AD, Wormit M, Cederbaum LS. 2011. Ultrafast charge separation driven by differential particle and hole mobilities. *J. Chem. Phys.* 134:024303
9. Beck AR, Bernhardt B, Warrick ER, Wu M, Chen S, et al. 2014. Attosecond transient absorption probing of electronic superpositions of bound states in neon: detection quantum beats. *New J. Phys.* 16:113016
10. Corkum PB, Krausz F. 2007. Attosecond science. *Nat. Phys.* 3:381–87
11. Leone SR, McCurdy CW, Burgdörfer J, Cederbaum LS, Chang Z, et al. 2014. What will it take to observe processes in "real time"? *Nat. Photonics* 8:162–66

12. Hentschel M, Kienberger R, Spielmann C, Reider GA, Milosevic N, et al. 2001. Attosecond metrology. *Nature* 414:509–13
13. Krause J, Schafer K, Kulander K. 1992. High-order harmonic generation from atoms and ions in the high intensity regime. *Phys. Rev. Lett.* 68:3535–38
14. Corkum PB. 1993. Plasma perspective on strong-field multiphoton ionization. *Phys. Rev. Lett.* 71:1994–97
15. Christov I, Murnane M, Kapteyn HC. 1997. High-harmonic generation of attosecond pulses in the "single-cycle" regime. *Phys. Rev. Lett.* 78:1251–54
16. Rundquist A, Durfee CG III, Chang Z, Herne C, Backus S, et al. 1998. Phase-matched generation of coherent soft X-rays. *Science* 280:1412–15
17. Ghimire S, DiChiara AD, Sistrunk E, DiMauro LF, Agostini P, Reis DA. 2011. Observation of high-order harmonic generation in a bulk crystal. *Nat. Phys.* 7:138–41
18. Vampa G, McDonald CR, Orlando G, Klug DD, Corkum PB, Brabec T. 2014. Theoretical analysis of high-harmonic generation in solids. *Phys. Rev. Lett.* 113:073901
19. Higuchi T, Stockman MI, Hommelhoff P. 2014. Strong-field perspective on high-harmonic radiation from bulk solids. *Phys. Rev. Lett.* 113:213901
20. Lewenstein M, Balcou P, Ivanov MY, L'Huillier A, Corkum PB. 1994. Theory of high-harmonic generation of low-frequency laser fields. *Phys. Rev. A* 49:2117
21. Colosimo P, Doumy G, Blaga CI, Wheeler J, Hauri C, et al. 2008. Scaling strong-field interactions towards the classical limit. *Nat. Phys.* 4:386–89
22. Doumy G, Wheeler J, Roedig C, Chirla R, Agostini P, DiMauro L. 2009. Attosecond synchronization of high-order harmonics from midinfrared drivers. *Phys. Rev. Lett.* 102:093002
23. Schmidt BE, Shiner AD, Giguère M, Lassonde P, Trallero-Herrero CA, et al. 2012. High harmonic generation with long-wavelength few-cycle laser pulses. *J. Phys. B* 45:074008
24. Popmintchev T, Chen M-C, Popmintchev D, Arpin P, Brown S, et al. 2012. Bright coherent ultrahigh harmonics in the keV X-ray regime from mid-infrared femtosecond lasers. *Science* 336:1287–91
25. Chen M-C, Mancuso C, Hernández-García C, Dollar F, Galloway B, et al. 2014. Generation of bright isolated attosecond soft X-ray pulses driven by multicycle midinfrared lasers. *PNAS* 111:E2361–67
26. Papadogiannis NA, Witzel B, Kalpouzos C, Charalambidis D. 1999. Observation of attosecond light localization in higher order harmonic generation. *Phys. Rev. Lett.* 83:4289–92
27. Paul PM, Toma ES, Breger P, Mullot G, Auge F, et al. 2001. Observation of a train of attosecond pulses from high harmonic generation. *Science* 292:1689–92
28. López-Martens R, Varjú K, Johnsson P, Mauritsson J, Mairesse Y, et al. 2005. Amplitude and phase control of attosecond light pulses. *Phys. Rev. Lett.* 94:033001
29. Jones DJ. 2000. Carrier-envelope phase control of femtosecond mode-locked lasers and direct optical frequency synthesis. *Science* 288:635–39
30. Goulielmakis E, Schultze M, Hofstetter M, Yakovlev VS, Gagnon J, et al. 2008. Single-cycle nonlinear optics. *Science* 320:1614
31. Kovačev M, Mairesse Y, Priori E, Merdji H, Tcherbakoff O, et al. 2003. Temporal confinement of the harmonic emission through polarization gating. *Eur. Phys. J. D* 26:79–82
32. Sansone G, Benedetti E, Calegari F, Vozzi C, Avaldi L, et al. 2006. Isolated single-cycle attosecond pulses. *Science* 314:443–46
33. Chini M, Zhao K, Chang Z. 2014. The generation, characterization and applications of broadband isolated attosecond pulses. *Nat. Photonics* 8:178–86
34. Pfeifer T, Gallmann L, Abel MJ, Neumark DM, Leone SR. 2006. Single attosecond pulse generation in the multicycle-driver regime by adding a weak second-harmonic field. *Opt. Lett.* 31:975
35. Chang Z. 2007. Controlling attosecond pulse generation with a double optical gating. *Phys. Rev. A* 76:051403
36. Mashiko H, Gilbertson S, Li C, Khan SD, Shakya MM, et al. 2008. Double optical gating of high-order harmonic generation with carrier-envelope phase stabilized lasers. *Phys. Rev. Lett.* 100:103906
37. Feng X, Gilbertson S, Mashiko H, Wang H, Khan SD, et al. 2009. Generation of isolated attosecond pulses with 20 to 28 femtosecond lasers. *Phys. Rev. Lett.* 103:28–31

38. Zhao K, Zhang Q, Chini M, Wu Y, Wang X, Chang Z. 2012. Tailoring a 67 attosecond pulse through advantageous phase-mismatch. *Opt. Lett.* 37:3891–93
39. Pfeifer T, Jullien A, Abel MJ, Nagel PM, Gallmann L, et al. 2007. Generating coherent broadband continuum soft-X-ray radiation by attosecond ionization gating. *Opt. Express* 15:17120
40. Abel MJ, Pfeifer T, Nagel PM, Boutu W, Bell MJ, et al. 2009. Isolated attosecond pulses from ionization gating of high-harmonic emission. *Chem. Phys.* 366:9–14
41. Vincenti H, Quéré F. 2012. Attosecond lighthouses: how to use spatiotemporally coupled light fields to generate isolated attosecond pulses. *Phys. Rev. Lett.* 108:113904
42. Pfeiffer AN, Cirelli C, Smolarski M, Dörner R, Keller U. 2011. Timing the release in sequential double ionization. *Nat. Phys.* 7:428–33
43. Pfeiffer AN, Cirelli C, Smolarski M, Keller U. 2013. Recent attoclock measurements of strong field ionization. *Chem. Phys.* 414:84–91
44. Eckle P, Smolarski M, Schlup P, Biegert J, Staudte A, et al. 2008. Attosecond angular streaking. *Nat. Phys.* 4:565–70
45. Gallmann L, Cirelli C, Keller U. 2012. Attosecond science: recent highlights and future trends. *Annu. Rev. Phys. Chem.* 63:447–69
46. Föhlisch A, Feulner P, Hennies F, Fink A, Menzel D, et al. 2005. Direct observation of electron dynamics in the attosecond domain. *Nature* 436:373–76
47. Wang L, Chen W, Wee ATS. 2008. Charge transfer across the molecule/metal interface using the core hole clock technique. *Surf. Sci. Rep.* 63:465–86
48. Friedlein R, Braun S, de Jong MP, Osikowicz W, Fahlman M, Salaneck WR. 2011. Ultra-fast charge transfer in organic electronic materials and at hybrid interfaces studied using the core-hole clock technique. *J. Electron Spectrosc. Relat. Phenom.* 183:101–6
49. Nabekawa Y, Shimizu T, Okino T, Furusawa K, Hasegawa H, et al. 2006. Interferometric autocorrelation of an attosecond pulse train in the single-cycle regime. *Phys. Rev. Lett.* 97:153904
50. Remetter T, Johnsson P, Mauritsson J, Varjú K, Ni Y, et al. 2006. Attosecond electron wave packet interferometry. *Nat. Phys.* 2:323–26
51. Johnsson P, Mauritsson J, Remetter T, L'Huillier A, Schafer KJ. 2007. Attosecond control of ionization by wave-packet interference. *Phys. Rev. Lett.* 99:233001
52. Holler M, Schapper F, Gallmann L, Keller U. 2011. Attosecond electron wave-packet interference observed by transient absorption. *Phys. Rev. Lett.* 106:123601
53. Lucchini M, Herrmann J, Ludwig A, Locher R, Sabbar M, et al. 2013. Role of electron wavepacket interference in the optical response of helium atoms. *New J. Phys.* 15:103010
54. Ott C, Kaldun A, Argenti L, Raith P, Meyer K, et al. 2014. Reconstruction and control of a time-dependent two-electron wave packet. *Nature* 516:374–78
55. Agostini P, DiMauro LF. 2004. The physics of attosecond light pulses. *Rep. Prog. Phys.* 67:813–55
56. Kling MF, Vrakking MJJ. 2008. Attosecond electron dynamics. *Annu. Rev. Phys. Chem.* 59:463–92
57. Pfeifer T, Abel MJ, Nagel PM, Jullien A, Loh Z-H, et al. 2008. Time-resolved spectroscopy of attosecond quantum dynamics. *Chem. Phys. Lett.* 463:11–24
58. Krausz F, Ivanov M. 2009. Attosecond physics. *Rev. Mod. Phys.* 81:163–234
59. Lépine F, Ivanov MY, Vrakking MJJ. 2014. Attosecond molecular dynamics: fact or fiction? *Nat. Photonics* 8:195–204
60. Krausz F, Stockman MI. 2014. Attosecond metrology: from electron capture to future signal processing. *Nat. Photonics* 8:205–13
61. Ghimire S, Ndabashimiye G, DiChiara AD, Sistrunk E, Stockman MI, et al. 2014. Strong-field and attosecond physics in solids. *J. Phys. B* 47:204030
62. Kim KT, Villeneuve DM, Corkum PB. 2014. Manipulating quantum paths for novel attosecond measurement methods. *Nat. Photonics* 8:187–94
63. Uiberacker M, Uphues T, Schultze M, Verhoef AJ, Yakovlev V, et al. 2007. Attosecond real-time observation of electron tunnelling in atoms. *Nature* 446:627–32
64. Schultze M, Fiess M, Karpowicz N, Gagnon J, Korbman M, et al. 2010. Delay in photoemission. *Science* 328:1658–62

65. Schultze M, Bothschafter EM, Sommer A, Holzner S, Schweinberger W, et al. 2013. Controlling dielectrics with the electric field of light. *Nature* 493:75–78
66. Schultze M, Ramasesha K, Pemmaraju CD, Sato SA, Whitmore D, et al. 2014. Ultrafast dynamics. Attosecond band-gap dynamics in silicon. *Science* 346:1348–52
67. Itatani J, Quéré F, Yudin GL, Ivanov MY, Krausz F, Corkum PB. 2002. Attosecond streak camera. *Phys. Rev. Lett.* 88:173903
68. Kienberger R, Goulielmakis E, Uiberacker M, Baltuška A, Yakovlev VS, et al. 2004. Atomic transient recorder. *Nature* 427:817–21
69. Mairesse Y, Quéré F. 2005. Frequency-resolved optical gating for complete reconstruction of attosecond bursts. *Phys. Rev. A* 71:011401
70. Drescher M, Hentschel M, Kienberger R, Uiberacker M, Yakovlev V, et al. 2002. Time-resolved atomic inner-shell spectroscopy. *Nature* 419:803–7
71. Cavalieri AL, Müller N, Uphues T, Yakovlev VS, Baltuška A, et al. 2007. Attosecond spectroscopy in condensed matter. *Nature* 449:1029–32
72. Neppl S, Ernstorfer R, Bothschafter EM, Cavalieri AL, Menzel D, et al. 2012. Attosecond time-resolved photoemission from core and valence states of magnesium. *Phys. Rev. Lett.* 109:87401
73. Kheifets AS, Ivanov IA. 2010. Delay in atomic photoionization. *Phys. Rev. Lett.* 105:233002
74. Baggesen JC, Madsen LB. 2010. Polarization effects in attosecond photoelectron spectroscopy. *Phys. Rev. Lett.* 104:043602
75. Moore LR, Lysaght MA, Parker JS, van der Hart HW, Taylor KT. 2011. Time delay between photoemission from the 2*p* and 2*s* subshells of neon. *Phys. Rev. A* 84:061404
76. Nagele S, Pazourek R, Feist J, Doblhoff-Dier K, Lemell C, et al. 2011. Time-resolved photoemission by attosecond streaking: extraction of time information. *J. Phys. B* 44:081001
77. Pazourek R, Feist J, Nagele S, Burgdörfer J. 2012. Attosecond streaking of correlated two-electron transitions in helium. *Phys. Rev. Lett.* 108:163001
78. Feist J, Zatsarinny O, Nagele S, Pazourek R, Burgdörfer J, et al. 2014. Time delays for attosecond streaking in photoionization of neon. *Phys. Rev. A* 89:033417
79. Mauritsson J, Remetter T, Swoboda M, Klünder K, L'Huillier A, et al. 2010. Attosecond electron spectroscopy using a novel interferometric pump-probe technique. *Phys. Rev. Lett.* 105:053001
80. Sansone G, Kelkensberg F, Pérez-Torres JF, Morales F, Kling MF, et al. 2010. Electron localization following attosecond molecular photoionization. *Nature* 465:763–66
81. Calegari F, Ayuso D, Trabattoni A, Belshaw L, De Camillis S, et al. 2014. Ultrafast electron dynamics in phenylalanine initiated by attosecond pulses. *Science* 346:336–39
82. Beck AR, Neumark DM, Leone SR. 2014. Probing ultrafast dynamics with attosecond transient absorption. *Chem. Phys. Lett.* 624:119–30
83. Pollard WT, Mathies RA. 1992. Analysis of femtosecond dynamic absorption spectra of nonstationary states. *Annu. Rev. Phys. Chem.* 43:497–523
84. Mukamel S. 1995. *Principles of Nonlinear Optical Spectroscopy*. New York: Oxford Univ. Press
85. Gaarde MB, Buth C, Tate JL, Schafer KJ. 2011. Transient absorption and reshaping of ultrafast XUV light by laser-dressed helium. *Phys. Rev. A* 83:013419
86. Chu W-C, Lin CD. 2012. Photoabsorption of attosecond XUV light pulses by two strongly laser-coupled autoionizing states. *Phys. Rev. A* 85:013409
87. Pfeiffer AN, Leone SR. 2012. Transmission of an isolated attosecond pulse in a strong-field dressed atom. *Phys. Rev. A* 85:053422
88. Pabst S, Sytcheva A, Moulet A, Wirth A, Goulielmakis E, Santra R. 2012. Theory of attosecond transient-absorption spectroscopy of krypton for overlapping pump and probe pulses. *Phys. Rev. A* 86:063411
89. Wirth A, Santra R, Goulielmakis E. 2013. Real time tracing of valence-shell electronic coherences with attosecond transient absorption spectroscopy. *Chem. Phys.* 414:149–59
90. Chen S, Bell MJ, Beck AR, Mashiko H, Wu M, et al. 2012. Light-induced states in attosecond transient absorption spectra of laser-dressed helium. *Phys. Rev. A* 86:063408
91. Bell MJ, Beck AR, Mashiko H, Neumark DM, Leone SR. 2013. Intensity dependence of light-induced states in transient absorption of laser-dressed helium measured with isolated attosecond pulses. *J. Mod. Opt.* 60:1506–16

92. Wu M, Chen S, Gaarde MB, Schafer KJ. 2013. Time-domain perspective on Autler-Townes splitting in attosecond transient absorption of laser-dressed helium atoms. *Phys. Rev. A* 88:043416
93. Chen S, Wu M, Gaarde MB, Schafer KJ. 2013. Quantum interference in attosecond transient absorption of laser-dressed helium atoms. *Phys. Rev. A* 87:033408
94. Bernhardt B, Beck AR, Li X, Warrick ER, Bell MJ, et al. 2014. High-spectral-resolution attosecond absorption spectroscopy of autoionization in xenon. *Phys. Rev. A* 89:023408
95. Ott C, Kaldun A, Raith P, Meyer K, Laux M, et al. 2013. Lorentz meets Fano in spectral line shapes: a universal phase and its laser control. *Science* 340:716–20
96. Wang H, Chini M, Chen S, Zhang C-H, He F, et al. 2010. Attosecond time-resolved autoionization of argon. *Phys. Rev. Lett.* 105:3–6
97. Cheng Y, Chini M, Wang X, Wu Y, Chang Z. 2014. *Attosecond transient absorption in molecular hydrogen*. Work. Pap. FM2B.3, CLEO 2014, Tech. Dig., Opt. Soc. Am.
98. Baker S, Robinson JS, Haworth CA, Teng H, Smith RA, et al. 2006. Probing proton dynamics in molecules on an attosecond time scale. *Science* 312:424–27
99. Kling MF, Siedschlag C, Verhoef AJ, Khan JI, Schultze M, et al. 2006. Control of electron localization in molecular dissociation. *Science* 312:246–48
100. Weinkauf R, Schanen P, Yang D, Soukara S, Schlag EW. 1995. Elementary processes in peptides: electron mobility and dissociation in peptide cations in the gas phase. *J. Phys. Chem.* 99:11255–65
101. Weinkauf R, Schanen P, Metsala A, Schlag EW, Burgle M, Kessler H. 1996. Highly efficient charge transfer in peptide cations in the gas phase: threshold effects and mechanism. *J. Phys. Chem.* 100:18567–85
102. Remacle F, Levine RD, Schlag EW, Weinkauf R. 1999. Electronic control of site selective reactivity: a model combining charge migration and dissociation. *J. Phys. Chem.* 103:10149–58
103. Cederbaum LS, Zobeley J. 1999. Ultrafast charge migration by electron correlation. *Chem. Phys. Lett.* 307:205–10
104. Kuleff AI, Cederbaum LS. 2007. Charge migration in different conformers of glycine: the role of nuclear geometry. *Chem. Phys.* 338:320–28
105. Lünnemann S, Kuleff AI, Cederbaum LS. 2008. Ultrafast charge migration in 2-phenylethyl-*N*,*N*-dimethylamine. *Chem. Phys. Lett.* 450:232–35
106. Kuleff AI, Lünnemann S, Cederbaum LS. 2010. Ultrafast charge migration following valence ionization of 4-methylphenol: jumping over the aromatic ring. *J. Phys. Chem. A* 114:8676–79
107. Dutoi AD, Wormit M, Cederbaum LS. 2011. Ultrafast charge separation driven by differential particle and hole mobilities. *J. Chem. Phys.* 134:024303
108. Kuleff AI, Lünnemann S, Cederbaum LS. 2012. Ultrafast reorganization of the hole charge created upon outer-valence ionization of porphyrins. *Chem. Phys.* 399:245–51
109. Kuleff AI, Lünnemann S, Cederbaum LS. 2013. Electron-correlation-driven charge migration in oligopeptides. *Chem. Phys.* 414:100–5
110. Kuleff AI, Cederbaum LS. 2014. Ultrafast correlation-driven electron dynamics. *J. Phys. B* 47:124002
111. Dutoi AD, Cederbaum LS. 2014. Time-resolved pump-probe spectroscopy to follow valence electronic motion in molecules: application. *Phys. Rev. A* 90:023414
112. Remacle F, Levine RD. 1999. Charge migration and control of site selective reactivity: the role of covalent and ionic states. *J. Chem. Phys.* 110:5089–99
113. Remacle F, Levine RD. 2006. An electronic time scale in chemistry. *PNAS* 103:6793–98
114. Remacle F, Kienberger R, Krausz F, Levine RD. 2007. On the feasibility of an ultrafast purely electronic reorganization in lithium hydride. *Chem. Phys.* 338:342–47
115. Periyasamy G, Levine RD, Remacle F. 2009. Electronic wave packet motion in water dimer cation: a many electron description. *Chem. Phys.* 366:129–38
116. Mignolet B, Levine RD, Remacle F. 2014. Charge migration in the bifunctional penna cation induced and probed by ultrafast ionization: a dynamical study. *J. Phys. B* 47:124011
117. Lehr L, Horneff T, Weinkauf R, Schlag EW. 2005. Femtosecond dynamics after ionization: 2-phenylethyl-*N*,*N*-dimethylamine as a model system for nonresonant downhill charge transfer in peptides. *J. Phys. Chem. A* 109:8074–80
118. Kuleff AI, Breidbach J, Cederbaum LS. 2005. Multielectron wave-packet propagation: general theory and application. *J. Chem. Phys.* 123:044111

119. Remacle F, Levine RD. 2006. The time scale for electronic reorganization upon sudden ionization of the water and water-methanol hydrogen bonded dimers and of the weakly bound no dimer. *J. Chem. Phys.* 125:133321
120. Dutoi AD, Gokhberg K, Cederbaum LS. 2013. Time-resolved pump-probe spectroscopy to follow valence electronic motion in molecules: theory. *Phys. Rev. A* 88:013419
121. Magerl E, Neppl S, Cavalieri AL, Bothschafter EM, Stanislawski M, et al. 2011. A flexible apparatus for attosecond photoelectron spectroscopy of solids and surfaces. *Rev. Sci. Instrum.* 82:063104
122. Ossiander M, Riemensberger J, Schäffer M, Gerl M, Schiffrin A, et al. 2014. Towards the absolute timing of photoemission from condensed matter systems. *J. Chem. Phys.* 141:144703
123. Stockman MI, Kling MF, Kleineberg U, Krausz F. 2007. Attosecond nanoplasmonic-field microscope. *Nat. Photonics* 1:539–44
124. Skopalová E, Lei DY, Witting T, Arrell C, Frank F, et al. 2011. Numerical simulation of attosecond nanoplasmonic streaking. *New J. Phys.* 13:083003
125. Prell JS, Borja LJ, Neumark DM, Leone SR. 2013. Simulation of attosecond-resolved imaging of the plasmon electric field in metallic nanoparticles. *Ann. Phys.* 525:151–61
126. Lemell C, Solleder B, Tőkési K, Burgdörfer J. 2009. Simulation of attosecond streaking of electrons emitted from a tungsten surface. *Phys. Rev. A* 79:062901
127. Zhang C-H, Thumm U. 2009. Attosecond photoelectron spectroscopy of metal surfaces. *Phys. Rev. Lett.* 102:123601
128. Kazansky A, Echenique P. 2009. One-electron model for the electronic response of metal surfaces to subfemtosecond photoexcitation. *Phys. Rev. Lett.* 102:177401
129. Zhang C-H, Thumm U. 2011. Effect of wave-function localization on the time delay in photoemission from surfaces. *Phys. Rev. A* 84:065403
130. Borisov A, Sánchez-Portal D, Kazansky A, Echenique P. 2013. Resonant and nonresonant processes in attosecond streaking from metals. *Phys. Rev. B* 87:121110
131. Schiffrin A, Paasch-Colberg T, Karpowicz N, Apalkov V, Gerster D, et al. 2013. Optical-field-induced current in dielectrics. *Nature* 493:70–74
132. Yabana K, Sugiyama T, Shinohara Y, Otobe T, Bertsch GF. 2012. Time-dependent density functional theory for strong electromagnetic fields in crystalline solids. *Phys. Rev. B* 85:045134
133. Prendergast D, Galli G. 2006. X-ray absorption spectra of water from first principles calculations. *Phys. Rev. Lett.* 96:215502
134. Shinohara Y, Yabana K, Kawashita Y, Iwata J-I, Otobe T, Bertsch GF. 2010. Coherent phonon generation in time-dependent density functional theory. *Phys. Rev. B* 82:155110
135. Spielmann C. 2014. Electrons take the fast track through silicon. *Science* 346:1293–94
136. Viña L, Cardona M. 1984. Effect of heavy doping on the optical properties and the band structure of silicon. *Phys. Rev. B* 29:6739–51
137. Worth GA, Cederbaum LS. 2004. Beyond born-oppenheimer: molecular dynamics through a conical intersection. *Annu. Rev. Phys. Chem.* 55:127–58
138. Tinkham M. 1996. *Introduction to Superconductivity*. Mineola, NY: Dover. 2nd ed.
139. Imada M, Fujimori A, Tokura Y. 1998. Metal-insulator transitions. *Rev. Mod. Phys.* 70:1039–1263
140. Pergament A. 2003. Metal-insulator transition: the Mott criterion and coherence length. *J. Phys. Condens. Matter* 15:3217
141. Cavalleri A, Rini M, Chong H, Fourmaux S, Glover T, et al. 2005. Band-selective measurements of electron dynamics in VO_2 using femtosecond near-edge X-ray absorption. *Phys. Rev. Lett.* 95:067405
142. Takahashi EJ, Lan P, Mücke OD, Nabekawa Y, Midorikawa K. 2013. Attosecond nonlinear optics using gigawatt-scale isolated attosecond pulses. *Nat. Commun.* 4:2691
143. Mukamel S, Healion D, Zhang Y, Biggs JD. 2013. Multidimensional attosecond resonant X-ray spectroscopy of molecules: lessons from the optical regime. *Annu. Rev. Phys. Chem.* 64:101–27

Annual Review of
Physical Chemistry
Volume 67, 2016

Contents

Indexes

Errata

An online log of corrections to *Annual Review of Physical Chemistry* articles may be found at http://www.annualreviews.org/errata/physchem